

Article

Influence of Anomalous Changes in the Crystal Structure on the Transport Properties of $\text{YbNi}_{1-x}\text{Cu}_x\text{Al}$ Series of Alloys

Daniel Rojas Pupo ^{1,*} , Flávio Guimarães Gandra ² and Luis Fernández Barquín ³ 

¹ Departamento de Estructuras y Física de Edificación, ETSAM, Universidad Politécnica de Madrid, 28040 Madrid, Spain

² Instituto de Física, Universidade Estadual de Campinas, Campinas 13083-970, Brazil; gandra@ifi.unicamp.br

³ Departamento CITIMAC, Facultad de Ciencias, Universidad de Cantabria, 39005 Santander, Spain; barquinl@unican.es

* Correspondence: d.rojas@upm.es; Tel.: +34-9106-7537

Abstract: Results of the transport properties of the $\text{YbNi}_{1-x}\text{Cu}_x\text{Al}$ ($x = 0, 0.2, 0.5, 0.8$ and 1.0) series of alloys are reported. The previous analysis of X-ray diffraction patterns indicates that all compounds crystallize in the hexagonal ZrNiAl structure with a linear behavior of the unit cell volume as a function of the Cu concentration (x). This is not found in the unit cell parameters, showing a discontinuity between $x = 0.5$ and 0.8 . Such discontinuities affect the behavior of the electrical resistivity, in which the position of the minimum temperature changes from 95 K to 175 K, and a rise in the low temperature slope in the magnetic contribution (with $-\ln T$ dependence) from $21 \mu\Omega\text{cm}$ to $212 \mu\Omega\text{cm}$ is observed. In addition, the electronic coefficient of the specific heat increases almost twofold from $125 \text{ mJ/mol}\cdot\text{K}^2$ ($x = 0.5$) to $246 \text{ mJ/mol}\cdot\text{K}^2$ ($x = 0.8$). These changes are attributed to the variation of the distance between Yb and transition metals (Ni and Cu) along the series and the different electronic properties of the transition metals (Ni and Cu).

Keywords: Yb alloys; intermediate valence; heavy fermion



Citation: Pupo, D.R.; Gandra, F.G.; Barquín, L.F. Influence of Anomalous Changes in the Crystal Structure on the Transport Properties of $\text{YbNi}_{1-x}\text{Cu}_x\text{Al}$ Series of Alloys. *Materials* **2022**, *15*, 1688. <https://doi.org/10.3390/ma15051688>

Academic Editor: Adam Grajcar

Received: 15 October 2021

Accepted: 21 February 2022

Published: 24 February 2022

Publisher's Note: MDPI stays neutral with regard to jurisdictional claims in published maps and institutional affiliations.



Copyright: © 2022 by the authors. Licensee MDPI, Basel, Switzerland. This article is an open access article distributed under the terms and conditions of the Creative Commons Attribution (CC BY) license (<https://creativecommons.org/licenses/by/4.0/>).

1. Introduction

The research on strongly correlated electron systems (SCES) occupies a relevant place within the areas of materials science research due to the rich phenomenology they present, connected directly to the understanding of the practical problem of mechanisms of high-temperature superconductivity [1]. Among them, Yb-based compounds have received special attention because of the variety of ground states which include magnetic, intermediate valence, and heavy fermion behaviors [2]. The nature of this ground state is established through a competition between the Kondo effect which favors a nonmagnetic ground state and the indirect magnetic intersite interaction between $4f$ local moments via the conduction electrons (Ruderman–Kittel–Kasuya–Yosida (RKKY)) interaction [3]. The balance between these two interactions can be tuned through the Jn_f parameter, where J is the coupling (exchange) between $4f$ and conduction electrons, and n_f is the density of states) with the application of pressure or by chemical substitution [1].

As a fine example, divalent Yb (nonmagnetic metal) under a pressure of 86 GPa becomes a superconductor before a stable trivalent (magnetic) state is reached, suggesting that magnetic instabilities may play a role in the appearance of superconductivity [4]. Another example is the antiferromagnetic YbCuGe , where the application of pressure induces a magnetic frustration in the triangular lattice of Yb ions of this compound [5]. On the other hand, the study of chemical substitution effects on the $\alpha\text{-YbAlB}_4$ system by Mn substitution at the Al site influences the intermediate valence state with the appearance of an antiferromagnetic transition at 20 K, a relatively high value for Yb compounds [6].

The present study focuses on the chemical substitution effects when Cu replaces Ni in the YbNiAl compound and the change in physical properties in the evolution toward

YbCuAl. Both compounds belong to a large class of intermetallic compounds of the type RTX (R—rare earth, T—transition metal, X—p element) [7]; in particular, those belonging to the YbTX series have attracted considerable interest in the past [8]. The YbCuAl alloy has been the subject of exhaustive studies because of the mixed-valence characteristics of Yb [9–13]. Such a system with an intermediate valence (IV) state presents a characteristic temperature T_f above which a local description of the $4f$ electrons seems applicable. However, below this temperature, an itinerant nonlocalized description is more adequate. According to the temperature dependence of the susceptibility for this alloy, the transition from the local (Curie–Weiss) high-temperature behavior to the nonlocal (T-independent Pauli-like) behavior occurs near $T_f = 30$ K [9,13]. The YbCuAl compound is also classified as a nonmagnetic CKS (concentrated Kondo system) with a high Kondo temperature value ($T_K = 66$ K), and an anomalous variation in temperature properties related to the formation of a narrow high-amplitude Abrikosov–Suhl resonance in the vicinity of the Fermi level [14]. Some studies have shown that, under a pressure of 8 GPa, the electrical resistivity curve shows an anomaly at 1 K, which has been interpreted as a sign of magnetic order [12]. Thus, the application of pressure, i.e., the unit cell volume reduction, favors the valence state 3^+ of the $4f^{13}$ configuration of Yb ions and, hence, the magnetic ordered state. Alternatively, chemical substitution effects in the $\text{Yb}_{1-x}\text{Y}_x\text{CuAl}$ series of alloys have indicated the expansion of the unit cell volume when Y replaces Yb. Thus, that chemical strategy is suitable for the study of negative pressure effects on YbCuAl, resulting in an increase in the Kondo interaction with the increase in Y concentration [13]. On the other hand, another archetypal system is YbNiAl, where a strong competition between Kondo and RKKY interactions leads to the formation of a magnetic ordered HF ground state, with an antiferromagnetic transition at $T_N = 3$ K [15]. Clearly, it appears attractive to follow the evolution of the physical properties from the antiferromagnetic YbNiAl system to the intermediate valence (nonmagnetic ground state) of the pure YbCuAl, in order to unveil the effect of this large difference on the behavior of these two archetypal alloys, as seen in the $\text{YbInNi}_{4-x}\text{Cu}_x$ series of alloys [16]. Special attention is paid to how the changes in the properties are connected with the above-introduced Jn_f parameter.

2. Materials and Methods

Samples of the $\text{YbNi}_{1-x}\text{Cu}_x\text{Al}$ (with $x = 0, 0.2, 0.5,$ and 1.0) series of alloys were prepared using a home-made arc-furnace, as used in the study of other Yb systems [13,16–18] and high-purity materials: Yb (99.9%), Ni (5 N), Cu (5 N), and Al (5 N) (Alfa-Johnson Matthey). Because of the high vapor pressure of Yb, small pieces of stoichiometric amounts of the materials were first pressed in a press pellet die with an excess of Yb (15–20%) to compensate for losses during fusion. The resulting ingots (of around 600 mg) were then melted three times to ensure homogeneity of the sample. During each step of melting, a loss of around 4–5% of Yb was observed. A subsequent annealing for 7 days of the resulting melting ingots at 750 °C was also carried out. In addition, reference (nonmagnetic) compounds $\text{YNi}_{1-x}\text{Cu}_x\text{Al}$ ($x = 0, 0.2, 0.5,$ and 1.0) were also prepared in the same setup in order to provide support to the analysis of the electrical resistivity data. X-ray diffraction patterns of the samples were recorded at 300 K in a Philips PW1710 diffractometer using CuK_α radiation ($\lambda = 1.5418$ Å) and a graphite secondary monochromator. The electrical resistivity (ρ) was measured using a standard four-probe dc method in a temperature range between 2 K and 300 K. The specific heat (c_p) was measured in a small sample calorimeter between 5 K and 30 K, using the thermal relaxation method, with the same experimental setup used in the study of other Yb series of alloys [13,16,17].

3. Results

3.1. X-ray Diffraction

The X-ray diffraction (XRD) patterns show the formation of the hexagonal ZrNiAl structure type for all samples of the series of $\text{YbNi}_{1-x}\text{Cu}_x\text{Al}$ and $\text{YNi}_{1-x}\text{Cu}_x\text{Al}$ alloys, as

shown in Figure 1a,b, respectively. For comparison and clarity purposes, the diffractograms of the different samples are shifted.

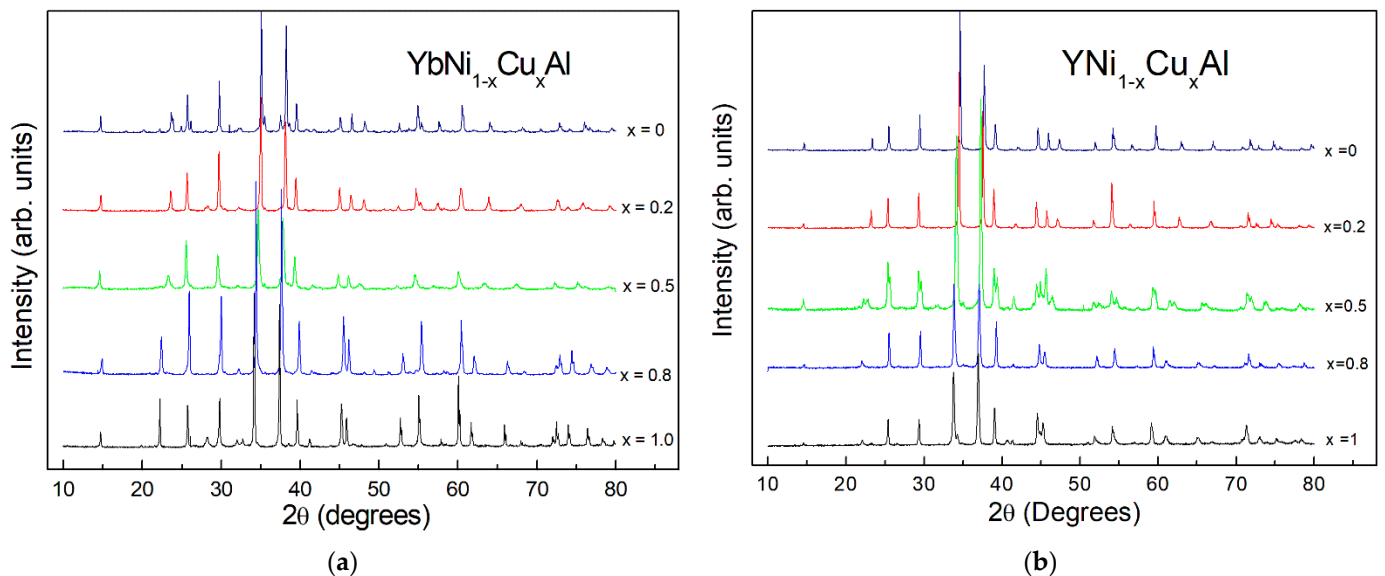


Figure 1. X-ray diffraction patterns of the $\text{YbNi}_{1-x}\text{Cu}_x\text{Al}$ (a) and $\text{YNi}_{1-x}\text{Cu}_x\text{Al}$ (b) series of alloys. All samples crystallize in a hexagonal ZrNiAl -type structure. The patterns of the different samples are shifted for comparison purposes.

The XRD patterns can be indexed according to the abovementioned type of structure, corresponding to the space group $P\bar{6}2m$. The values of the crystallographic unit cell parameters were obtained using the Rietveld method implemented in the Fullprof suite programs [19]. The results of the Rietveld refinement of the XRD data are presented in Table 1 for the $\text{YbNi}_{1-x}\text{Cu}_x\text{Al}$ series and in Table 2 for the $\text{YNi}_{1-x}\text{Cu}_x\text{Al}$ series. The refinements show a reasonable reliability with standard Bragg factors (R_B) between 10% and 15%. The lattice parameters calculated for YbCuAl ($x = 1$) were $a = 6.9360$ (6) Å and $c = 4.0044$ (4) Å, while those calculated for YbNiAl ($x = 0$) were $a = 6.9610$ (6) Å and $c = 3.7743$ (4) Å. These are in excellent agreement with those reported in the literature [9,10,15]. The unit cell volume values were also calculated ($V = a^2 c \sin 60^\circ$, for hexagonal lattices), as presented for both series (Tables 1 and 2). In the case of the Yb alloys, a small fraction (less than 5%) of YbAl_2 [20] and antiferromagnetic Yb_2O_3 ($T_N = 2.1$ K) was found. The nonmagnetic characteristics of YbAl_2 and the very low Néel transition ($T_N = 2.1$ K) of the antiferromagnetic Yb_2O_3 did not affect the interpretation of the properties of the main phase. It should be noted that the presence of a small fraction of Yb_2O_3 is commonly found in Yb alloys, appearing even in single crystals [13,21,22].

Table 1. Lattice parameters (a , c) and volume (V) as calculated by Rietveld refinements of the X-ray diffraction data of the $\text{YbNi}_{1-x}\text{Cu}_x\text{Al}$ series of alloys.

$\text{YbNi}_{1-x}\text{Cu}_x\text{Al}$	a (Å)	c (Å)	V (Å ³)
$x = 0$	6.9610 (6)	3.7743 (4)	158.38 (4)
$x = 0.2$	6.9823 (4)	3.7863 (3)	159.86 (3)
$x = 0.5$	7.002 (1)	3.8355 (8)	162.85 (8)
$x = 0.8$	6.9139 (5)	3.9883 (3)	165.11 (4)
$x = 1.0$	6.9360 (6)	4.0044 (4)	166.83 (5)

Table 2. Lattice parameters (a, c) and volume (V) as calculated by Rietveld refinements of the X-ray diffraction data of the $\text{YNi}_{1-x}\text{Cu}_x\text{Al}$ series of alloys.

$\text{YNi}_{1-x}\text{Cu}_x\text{Al}$	a (Å)	c (Å)	V (Å ³)
x = 0	7.0451 (5)	3.8450 (3)	165.28 (4)
x = 0.2	7.0641 (5)	3.8582 (3)	166.73 (4)
x = 0.5	7.0588 (8)	3.9287 (6)	169.53 (6)
x = 0.8	7.0169 (6)	4.0377 (5)	172.17 (5)
x = 1.0	7.0461 (5)	4.0382 (3)	173.63 (4)

As an example, the Rietveld refinement of $x = 0.8$ is presented in Figure 2. A good reliability of the fit is obtained with a Bragg factor ($R_B = 10.4\%$). Vertical markers indicate the positions of the peaks of the main phase (96.5 (7)%) and impurity phases: YbAl_2 (1.2%) and Yb_2O_3 (2.3%). The crystallographic structure of $x = 0.8$ consisted of planes of Yb, Ni, and Cu atoms between two others of Al, Ni, and Cu, with the Cu and Ni statistically distributed according to the ratio Ni (20%) and Cu (80%) (see inset of Figure 2).

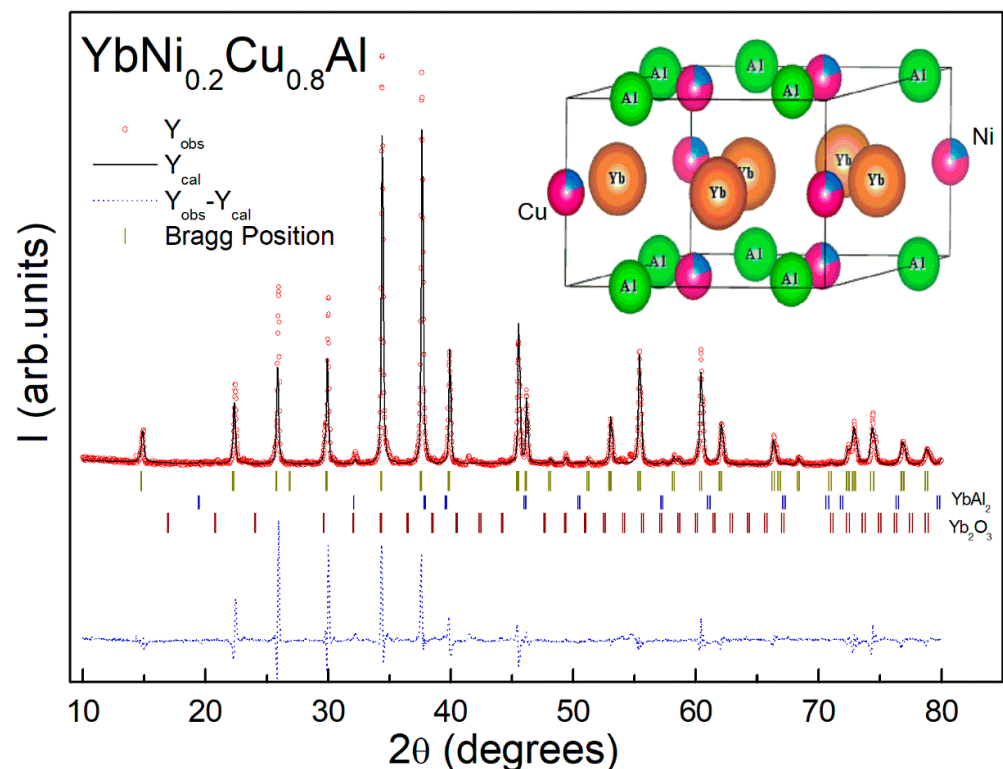


Figure 2. XRD pattern and Rietveld refinement in a representative Yb sample with $x = 0.8$. A good reliability of the fit is observed, with a standard Bragg factor ($R_B = 10.4\%$). Bragg positions (vertical markers) of the main phase and impurity phases (YbAl_2 and Yb_2O_3) are also provided. The scheme of the typical structure (inset) with the distribution of the different atoms is shown.

For the sake of clarity, the variation of the lattice parameters and the unit cell volume along the series as a function of the Cu concentration (x) is presented in Figure 3b. Interestingly, despite a linear variation (increase) of the unit cell volume with increasing Cu concentration (x), as found in other chemically substituted series of alloys [9,13,16,17], here, an anomalous variation of the lattice parameters was found (see Figure 3a). Indeed, for $x = 0.8$ and $x = 1$, a deviation from the general trend of $x = 0, 0.2$, and 0.5 alloys is observed. This anomaly cannot be attributed to changes in the valence with the Cu dilution upon going to the intermediate valence system YbCuAl , as the same behavior is found in the nonmagnetic counterpart $\text{YNi}_{1-x}\text{Cu}_x\text{Al}$ series of alloys, as depicted in Figure 3. It is de-

scribed below that the anomalous variation of the lattice parameters may have implications on the physical properties.

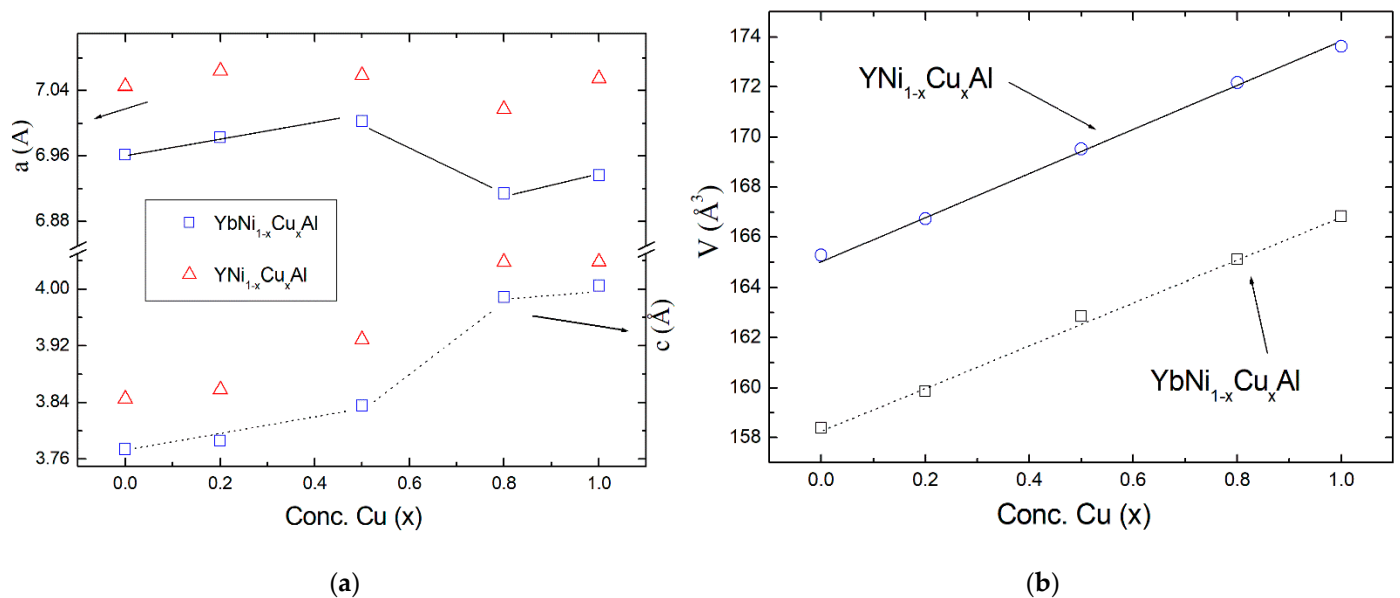


Figure 3. (a) Lattice a , c parameters vs. Cu concentration (x) in the series of $\text{YbNi}_{1-x}\text{Cu}_x\text{Al}$ and reference $\text{YNi}_{1-x}\text{Cu}_x\text{Al}$ compounds. There is an abrupt deviation from the linear behavior between $x = 0.5$ and 0.8 . (b) Unit cell volume vs. Cu concentration (x) variation following a linear behavior. Error bars (not indicated) are within the size of data points (see Tables 1 and 2).

3.2. Electrical Resistivity

In Figure 4, the results of the measurements of the electrical resistivity for all samples normalized to the value at 300 K ($\rho/\rho_{300\text{K}}$) are presented. The sample with $x = 1$ displays a different behavior with respect to the rest of the samples, with a characteristic decrease in the resistivity at lower temperatures according to a Kondo lattice system [13]. The remaining samples show a typical single-impurity Kondo behavior with the presence of a minimum and an abrupt increase in the resistivity on going to lower temperatures. The minimum associated with the Kondo effect is indicated by an arrow (and its temperature value, T_{min}). Interestingly, there is a trend marking a decrease from $x = 0$ to $x = 0.5$, which is broken for $x = 0.8$. The possible causes of this behavior are discussed below.

The electrical resistivity of isostructural compounds $\text{YNi}_{1-x}\text{Cu}_x\text{Al}$ shows a typical metallic behavior according to the Bloch–Grüneisen law, similar to that reported for YCuAl ($x = 1$) alloy [13]. To extract the magnetic contribution ρ_{mag} vs. temperature in the Yb-based series $\text{YbNi}_{1-x}\text{Cu}_x\text{Al}$, the resistivity of the nonmagnetic Y-based counterparts was subtracted, as presented in Figure 5. The resulting curves display two regions with $-\ln T$ dependence, characteristic of a Kondo interaction in the presence of crystalline field effects [16,17,23,24]. In hexagonal symmetry, the eightfold degenerate state of the Yb^{3+} ion with $J = 7/2$ is expected to split into four doublets [25]. The ratio of the high- and low-temperature slopes for $x = 0.5$ compound is around 5.1. This fact is consistent with a doublet ground state and a doublet excited state according to the Cornut–Coqblin model developed for Ce compounds [16,17,23,24]. However, for $x = 0.8$, the ratio is around 1.2, which indicates that this model could partially fail for the case of Yb-based alloys or additional effects must be taken into account [17,23]. The presence of crystalline field effects is clearly visible with a hump around 60 K (regions where the two slopes separate each other), which further indicates the splitting of the first excited state around 90 K [24]. For $x = 0$, a maximum around 3 K with a decrease below this temperature is associated with the AFM order [15].

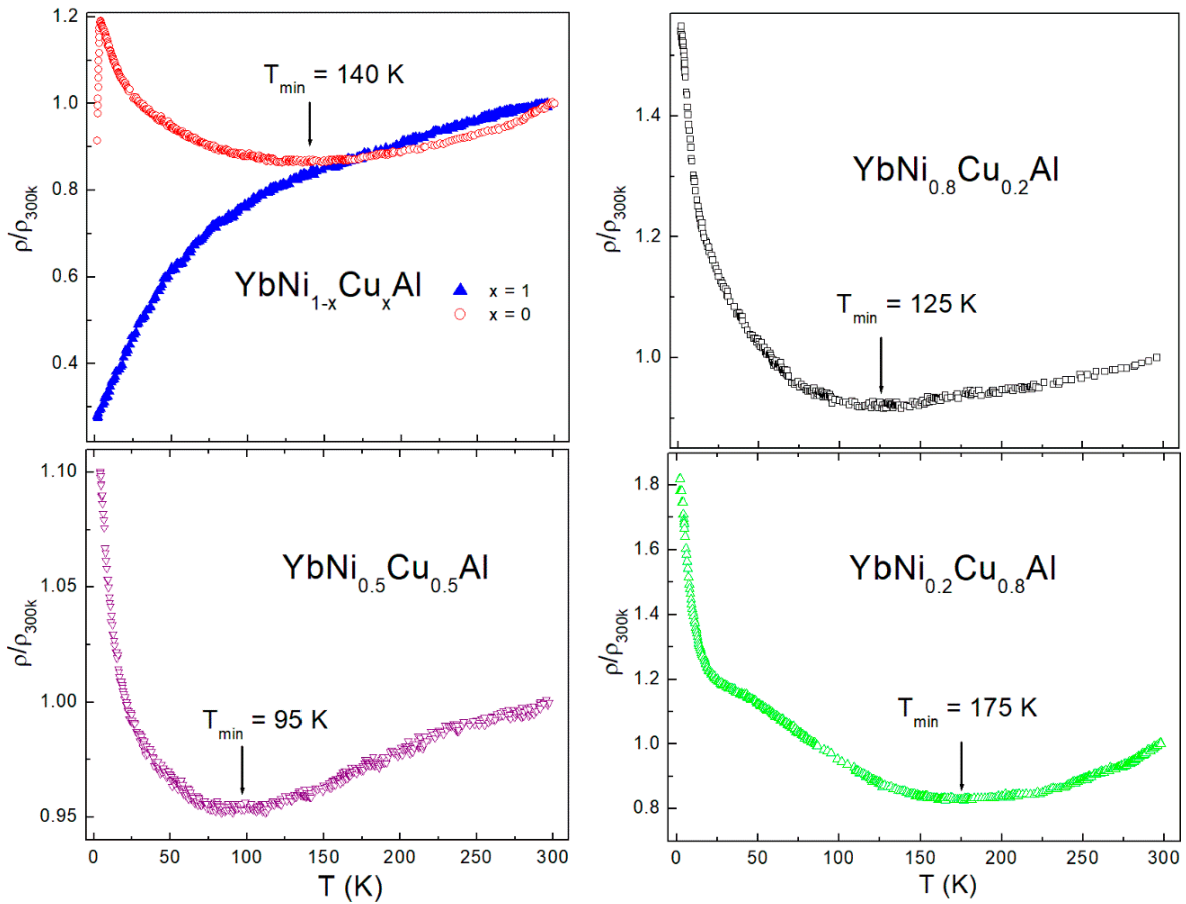


Figure 4. Temperature dependence of the electrical resistivity of the $\text{YbNi}_{1-x}\text{Cu}_x\text{Al}$ series of alloys in normalized form ($\rho/\rho_{300\text{K}}$). The minimum in the electrical resistivity associated with the Kondo effect is marked with an arrow, except for $x = 1$, where a Kondo lattice behavior is observed.

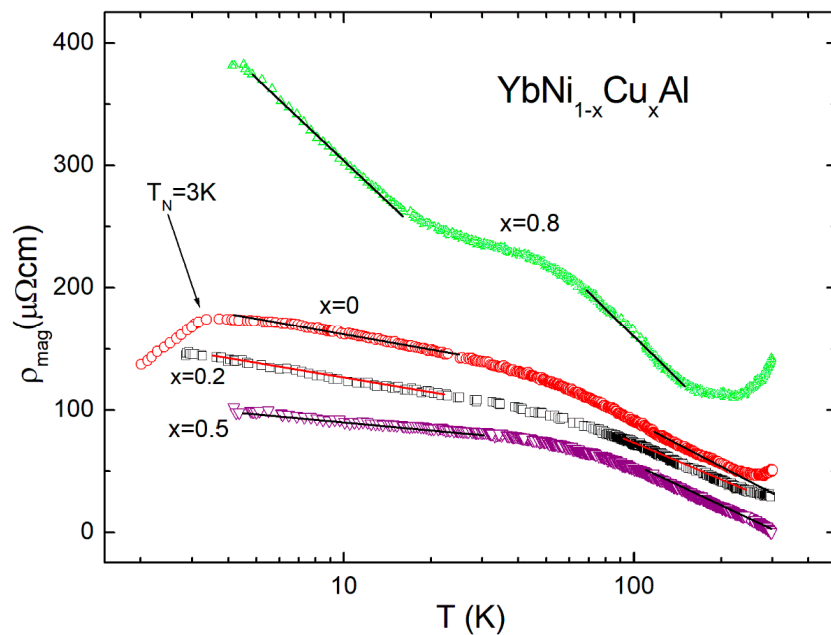


Figure 5. Magnetic contribution vs. temperature (in logarithmic scale) obtained by subtraction of the experimental data in $\text{YbNi}_{1-x}\text{Cu}_x\text{Al}$ alloys using reference $\text{YNi}_{1-x}\text{Cu}_x\text{Al}$ series. Two regions with $-\ln T$ dependence are observed.

3.3. Specific Heat

In Figure 6a, a plot of c_p/T vs. T is shown for the samples of the series $\text{YbNi}_{1-x}\text{Cu}_x\text{Al}$ in the low temperature range ($T < 30$ K).

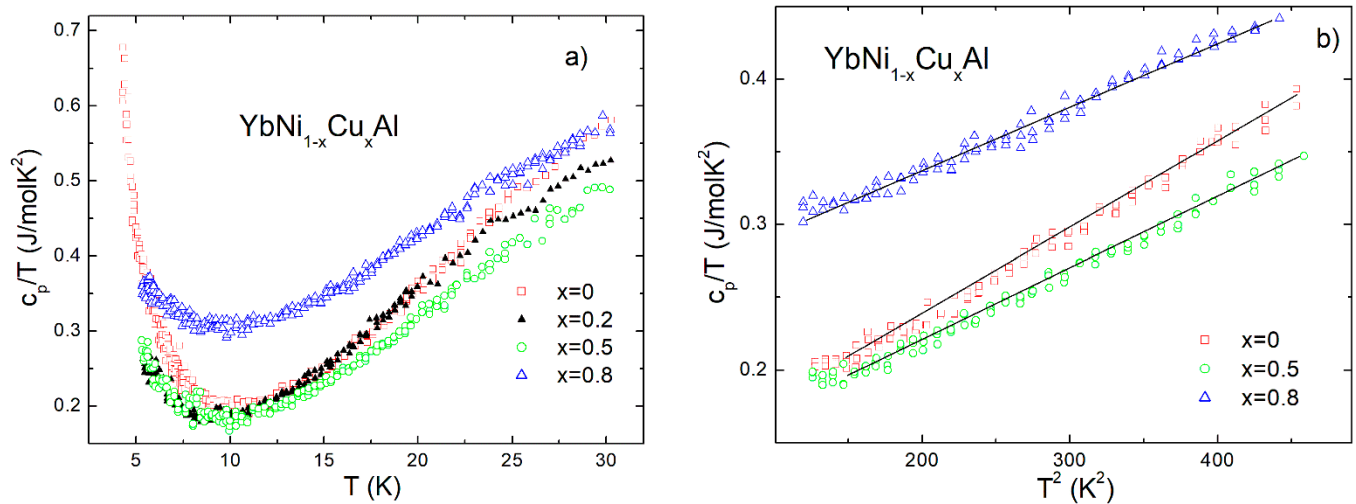


Figure 6. (a) c_p/T vs. temperature dependence in the $\text{YbNi}_{1-x}\text{Cu}_x\text{Al}$ series of alloys. The onset of competition between magnetic correlations and the Kondo effect below the minimum around 10 K is observed. (b) Plot of c_p/T vs. T^2 dependence showing a linear behavior in the temperature range between 11 K and 20 K.

The minimum around 10 K indicates the interplay of the competition between RKKY interaction and the Kondo effect on going to low temperatures [17,23], as indicated by electrical resistivity measurements (Figures 4 and 5). Above this temperature and up to 20 K, the c_p/T vs. T^2 dependence displays a linear behavior, which is in agreement with a $c_p \approx \gamma T + \beta T^3$ specific heat dependence for metals [13] (γ and β are related to the electronic and phonon contributions, respectively) as shown in Figure 6b. For the sake of clarity, the data of the $x = 0.2$ sample are not shown. Neglecting the influence of crystalline field effects, the estimate of the electronic coefficient gives close values around 117 mJ/mol·K² for $x = 0, 0.2,$ and 0.5 . However, an abrupt γ -increase for $x = 0.8$ (246 mJ/mol·K²) is observed. The probable causes of this striking behavior are discussed in detail in the next section.

4. Discussion

The joint analysis of the X-ray diffraction, electrical resistivity, and specific heat results on the $\text{YbNi}_{1-x}\text{Cu}_x\text{Al}$ alloys shown above allows discussing in detail the overall behavior of the samples. It is possible to relate the changes in the electrical transport and the thermal properties with the behavior of the lattice parameters upon Cu substitution (summarized in Table 3). As presented in Figure 3, there is an abrupt change between $x = 0.5$ and 0.8 in the lattice parameters, which can be basically associated with the Cu substitution by Ni and not to the change in the valence, because a similar change also appears in the nonmagnetic counterpart $\text{YNi}_{1-x}\text{Cu}_x\text{Al}$ series. These variations in the crystallographic structure are reflected in the other properties. For instance, the position in temperature of the minimum in the electrical resistivity, a fingerprint of the Kondo effect, (T_{min} , see Figure 4 and Table 3) decreases with the increase in Cu content from $x = 0$ to $x = 0.5$. Such a tendency is broken for $x = 0.8$, where an abrupt increase from 95 K to 175 K is observed. A similar trend can be deduced from the low-temperature slope (parameter C in Table 3), associated with Kondo behavior with a characteristic $-\ln T$ dependence. This is deduced from the analysis of the magnetic contribution of the electrical resistivity on the $\text{YbNi}_{1-x}\text{Cu}_x\text{Al}$ series of alloys (see Figure 5).

Table 3. Dependence on the Cu concentration (x) of some parameters extracted from the electrical resistivity and specific heat results in the series of YbNi_{1-x}Cu_xAl alloys.

YbNi _{1-x} Cu _x Al	T _{min} (K) (±10%)	C (μΩcm) (±1%)	γ (mJ/mol·K ²) (±1%)
x = 0	140	46	113
x = 0.2	128	39	114
x = 0.5	95	21	125
x = 0.8	175	212	246
x = 1	-	-	340

Moreover, the estimate of the electronic coefficient from the analysis of the specific heat data, particularly from the c_p/T vs. temperature curves (Figure 6b), is also in agreement with the tendency observed in the two mentioned parameters: T_{\min} and C (Table 3). Additionally, this increase in γ value may also be due to the influence of the electronic effects, as the substitution of Ni by Cu leads to an increase in the number of conduction electrons [16,26,27].

Additionally, the change in the hybridization between $4f$ electrons with the d -conduction band of transition metals Ni and Cu or p -band of Al must also play a significant role, as observed in CeNi_{1-x}Cu_x series of alloys [26,27]. According to the Wolf–Schrieffer transformation, a direct relation can be established between the Kondo coupling constant (J) of $4f$ and conduction electrons and the hybridization [14]. Moreover, as the Kondo temperature is related to the coupling constant (J) and the density of states at the Fermi level (n_f) as $T_K \approx \exp(-1/Jn_f)$, an increase in the hybridization or in the Jn_f product leads to an increase in the Kondo interactions. Since the strength of this hybridization between $4f$ and conduction electrons in YbNi_{1-x}Cu_xAl series of alloys depends on the distance between Yb and transition metal (Ni, Cu) or Al atoms, it is productive to follow how these distances change with the variation of the Cu concentration (x) along the series. These distances can be derived from the variation of the lattice parameters, obtained by the analysis of the X-ray diffraction data (Tables 1 and 2, Figure 3). In this sense, in Figure 7a, the dependence of the distance between Yb and transition metals ($d_{Yb-(Ni,Cu)}$) and Al (d_{Yb-Al}) as a function of the Cu concentration (x) is presented. It is observed that d_{Yb-Al} varies linearly with the change in the Cu concentration for all the studied samples between $x = 0$ and $x = 1$, just as the unit cell volume does (Figure 3). However, $d_{Yb-(Ni,Cu)}$ suffers an abrupt change around $x = 0.7$, which is similar to that observed in the parameters presented in Table 3. This indicates that a direct relation between the change in this distance $d_{Yb-(Ni,Cu)}$ and some parameters reflecting the variation in the Kondo interactions with the Cu alloying can be established, i.e., the minimum of the electrical resistivity (T_{\min}), as depicted in Figure 7b. This further indicates that, despite the substitution of Ni by Cu potentially provoking an increase in the density of states as a result of electronic effects [16,26,27], there is also a contribution of the structural changes along the series basically affecting the $4f-d$ hybridization. Therefore, the strength of Kondo interactions is equally affected. In fact, this is supported by the change in the low-temperature slope (C) in the magnetic contribution to the electrical resistivity (Table 3) since $C \approx J^3 n_f^2$ [17,23,24]. This indicates that the evolution from a magnetic behavior for $x = 0$ (Ni-side) to nonmagnetic HF state for $x = 1$ (Cu-side) is favored with the increase in Cu concentration (x). This situation is similar to that observed in other Ni–Cu-substituted series of alloys, such as Yb(Cu_{1-x}Ni_x)₂Si₂, where the magnetism is favored for high Ni concentrations, and the Kondo temperature is found to decrease on going to the Ni side [28].

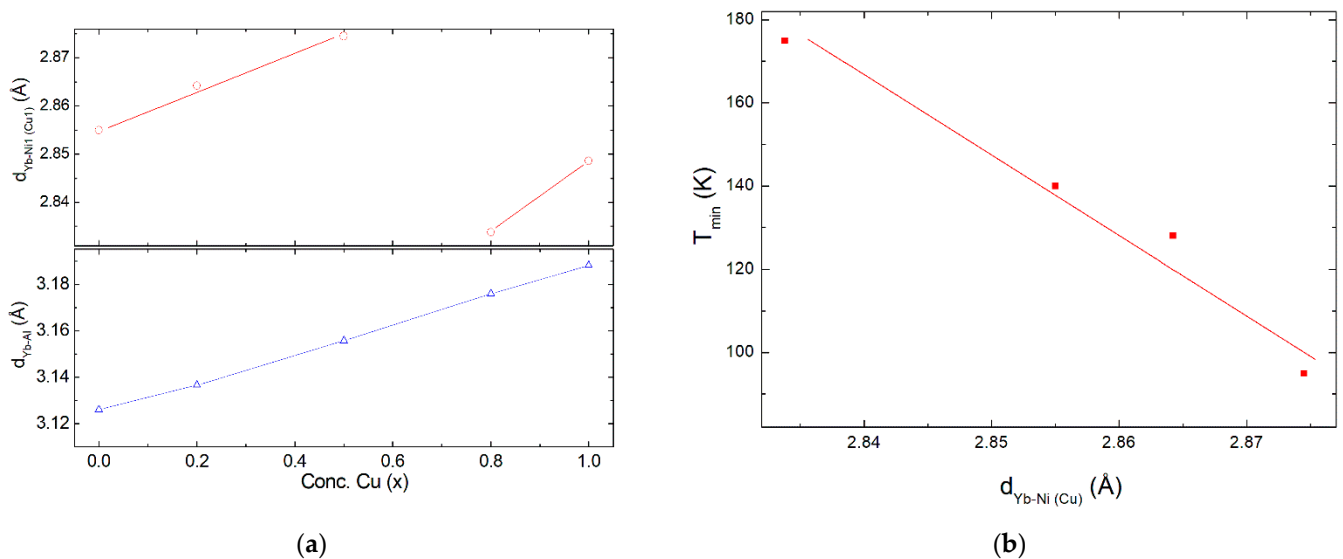


Figure 7. (a) Dependence of the distance between Yb and transition-metal atoms (Ni and Cu) ($d_{\text{Yb-Ni(Cu)}}$) and Al atom ($d_{\text{Yb-Al}}$) as a function of the Cu concentration (x). (b) Temperature of the minimum in the electrical resistivity vs. $d_{\text{Yb-Ni(Cu)}}$. A simple correlation between both parameters is found.

Another example was found when Cu replaces Ni in ferromagnetic YbInNi₄ (YbInNi_{4-x}Cu_x series). In this case, the magnetism disappears on going to the Cu side [16]. Thus, considering the above results, for Yb systems, it can be concluded that the RKKY interaction is favored in Ni compounds displaying a magnetic ordering, whereas, in Cu compounds, a nonmagnetic state would be dominant [18]. On the other hand, in Ce compounds, an inverse situation is found; a magnetic state is favored for Cu-rich compounds and the nonmagnetic state is favored for the CeNi one, as observed, for instance, in the studies of CeNi_{1-x}Cu_x [26,27] and CeNi_{1-x}Cu_xAl [29] series of alloys. In particular, in CeNi_{1-x}Cu_x series, a transition from the nonmagnetic state in CeNi to ferromagnetic state for $0.3 \leq x < 0.8$ and antiferromagnetic state for CeCu ($x = 1$) was reported [26]. In the CeNi_{1-x}Cu_xAl series of alloys with $x = 0, 0.05, 0.1, 0.2,$ and 0.3 , a smooth transition between the mixed-valence (nonmagnetic) state of CeNiAl to a trivalent state (Ce³⁺) with the Ni substitution by Cu was observed [29]. It is worth commenting that, in contrast to these chemically substituted studies in Ce alloys and in YbInNi_{4-x}Cu_x series [16], where both the lattice parameters and unit cell volume evolve continuously, the present YbNi_{1-x}Cu_xAl series showcases an abrupt variation of the lattice parameters with the Cu substitution.

5. Conclusions

A study on the influence of chemical substitution effects when Cu replaces Ni in the antiferromagnetic YbNiAl alloy (YbNi_{1-x}Cu_xAl series of alloys) was performed. The analysis of the X-ray diffraction data indicates an anomalous change in the unit cell parameters around $x = 0.7$, despite a common linear overall behavior of the unit cell volume. The presence of such abrupt changes contrasts the observations in most systems where a chemical substitution is performed [9,13,16–18]. In particular, the variation of the distance between Yb and transition metals (Ni,Cu) ($d_{\text{Yb-(Ni,Cu)}}$) is indicated as the main cause affecting the variation of the minimum of the electrical resistivity (T_{min}), of the low-temperature slope in the magnetic contribution to the electrical resistivity (C), and of the electronic coefficient (γ) of the specific heat as a function of the Cu concentration (x). This clearly indicates that, although an influence of electronic effects with the increase in the density of states when Cu replaces Ni is surely present, the hybridization between $4f$ and d -band conduction electrons would play the main role in changes of the physical properties along the YbNi_{1-x}Cu_xAl series. Thus, the evolution from the magnetic behavior of YbNiAl to a nonmagnetic HF state

of the YbCuAl system would be driven by a strong competition between the RKKY and Kondo effect, depending basically on the $4f$ – $3d$ hybridization, due to the variations in the crystallographic structure. In this context, it would be interesting to conduct electron spin resonance measurements to analyze the variation of the Yb-conduction electron exchange parameter J_{Yb} , similar to what has been done in the $Y_{1-x}Yb_xInNi_4$ series of alloys [18]. Furthermore, it would be interesting to extend this kind of study to other Yb systems, for instance, in the YbNi₂ binary alloy displaying ferromagnetism and HF behavior [30], through the YbNi_{2-x}Cu_x series of alloys.

Author Contributions: Conceptualization, all authors; methodology, all authors; validation, all authors; formal analysis, D.R.P.; investigation, all authors; writing—original draft preparation, D.R.P. and L.F.B.; writing—review and editing, all authors; visualization, D.R.P.; supervision, F.G.G.; project administration, D.R.P. and F.G.G.; funding acquisition, F.G.G. All authors have read and agreed to the published version of the manuscript.

Funding: This research was funded by the FAPESP Sao Paulo research foundation, grant number 1998/10011-8.

Institutional Review Board Statement: Not applicable.

Informed Consent Statement: Not applicable.

Data Availability Statement: Not applicable.

Conflicts of Interest: The authors declare no conflict of interest. The founders had no role in the design of the study; in the collection, analyses, or interpretation of data; in the writing of the manuscript, or in the decision to publish the results.

References

1. Paschen, S.; Si, Q. Quantum phases driven by strong correlations. *Nat. Rev. Phys.* **2021**, *3*, 9–26. [[CrossRef](#)]
2. Hewson, A.C. *The Kondo Problem to Heavy Fermions (Cambridge Studies on Magnetism)*, 1st ed.; Cambridge University Press: London, UK, 1993.
3. Doniach, S. The Kondo lattice and weak antiferromagnetism. *Physica B+C* **1977**, *91*, 231. [[CrossRef](#)]
4. Song, J.; Fabbri, G.; Bi, W.; Haskel, D.; Schilling, J.S. Pressure-Induced Superconductivity in Elemental Ytterbium Metal. *Phys. Rev. Lett.* **2018**, *121*, 037004. [[CrossRef](#)] [[PubMed](#)]
5. Umeo, K.; Watanabe, D.; Araki, K.; Katoh, K.; Takabatake, T. Uniaxial-Pressure-Induced Release of Magnetic Frustration in a Triangular Lattice Antiferromagnet YbCuGe. *Metals* **2021**, *11*, 30. [[CrossRef](#)]
6. Suzuki, S.; Takubo, K.; Kuga, K.; Higemoto, W.U.; Ito, T.; Tomita, T.; Shimura, Y.; Matsumoto, Y.; Bareille, C.; Wadati, H.; et al. High-temperature antiferromagnetism in Yb based heavy fermion systems proximate to a Kondo insulator. *Phys. Rev. Res.* **2021**, *3*, 023140. [[CrossRef](#)]
7. Gupta, S.; Suresh, K.G. Review on magnetic and related properties of RTX compounds. *J. Alloys Compd.* **2015**, *618*, 522–606. [[CrossRef](#)]
8. Pottgen, R.B.; Johrend, D.; Kubmann, D. Structure-property relations of ternary equiatomic YbTX intermetallics. In *Handbook on the Physics and Chemistry of Rare Earths*, 1st ed.; Gschneidner, K.A., Jr., Eyring, L., Lander, G.H., Eds.; Elsevier: Amsterdam, The Netherlands, 2001; Volume 32, pp. 453–506.
9. Mattens, W.C.M.; de Chatel, P.F.; Moleman, A.C.; de Boer, F.R. Intermediate-valence state of Yb in Y- and Gd substituted YbCuAl. *Physica B* **1979**, *96*, 138–143. [[CrossRef](#)]
10. Mattens, W.C.M.; Hölscher, H.; Tuin, G.J.M.; Moleman, A.C.; de Boer, F.R. Thermal expansion and magneto-volume effects in the mixed-valent compound YbCuAl. *J. Magn. Magn. Mater.* **1980**, *15*, 982–984. [[CrossRef](#)]
11. Pott, R.; Schefzyk, R.; Wohlleben, D.; Junod, A. Thermal expansion and specific heat of intermediate valent YbCuAl. *Z. Phys. B* **1981**, *44*, 17–24. [[CrossRef](#)]
12. Alami-Yadri, K.; Wilhelm, H.; Jaccard, D. Electrical resistivity of YbAuIn₂ and YbCuAl up to 8 GPa. *Solid State Commun.* **1998**, *108*, 279–283. [[CrossRef](#)]
13. Rojas, D.P.; Gandra, F.G.; Medina, A.N.; Fernández Barquín, L.; Gomez Sal, J.C. Kondo temperature and Heavy fermion behavior in Yb_{1-x}Y_xCuAl series of alloys. *Physica B* **2018**, *536*, 176–181. [[CrossRef](#)]
14. Brandt, N.; Moshchalkov, V.V. Concentrated Kondo Systems. *Adv. Phys.* **1984**, *33*, 373–467. [[CrossRef](#)]
15. Schank, C.; Olesch, G.; Kohler, J.; Tegel, U.; Klinger, U.; Diehl, J.; Klimm, S.; Sparr, G.; Horn, S.; Geibel, C.; et al. YbNiAl: A new Yb-based heavy fermion antiferromagnet. *J. Magn. Magn. Mater.* **1995**, *140*, 1237–1238. [[CrossRef](#)]
16. Rojas, D.P.; Medina, A.N.; Gandra, F.G.; Cardoso, L.P. Transport and thermodynamic properties of YbInNi_{4-x}Cu_x system. *J. Magn. Magn. Mater.* **2001**, *226*, 72–74. [[CrossRef](#)]

17. Rojas, D.P.; Cardoso, L.P.; Coelho, A.A.; Gandra, F.G.; Medina, A.N. Unusual behavior of the Kondo temperature of $\text{La}_{1-x}\text{Yb}_x\text{Cu}_3\text{Al}_2$. *Phys. Rev. B* **2001**, *63*, 165114. [[CrossRef](#)]
18. Medina, A.N.; Rojas, D.P.; Gandra, F.G. ESR of Gd^{3+} in $\text{Y}_{1-x-y}\text{Yb}_x\text{Gd}_y\text{InNi}_4$. *J. Magn. Magn. Mater.* **2001**, *226*, 77–79. [[CrossRef](#)]
19. Rodríguez-Carvajal, J. Recent advances in magnetic structure determination by neutron powder diffraction. *Physica B* **1993**, *192*, 55–69. [[CrossRef](#)]
20. Görlach, T.; Pfleiderer, C.; Grube, K.; Löhneysen, H.V. Low-temperature properties of YbAl_2 . *Phys. Rev. B* **2005**, *71*, 033101. [[CrossRef](#)]
21. Rojas, D.P.; Espeso, J.I.; Fernández Barquín, L.; Rodríguez Fernández, J. Reduction of the Yb valence in YbAl_3 nanoparticles. *Phys. Rev. B* **2008**, *78*, 094412. [[CrossRef](#)]
22. Hiess, A.; Boucherle, J.X.; Givord, F.; Canfield, P.C. Magnetic susceptibility and magnetization measurements of an YbAl_3 single crystal for groundstate investigations. *J. Alloys Compd.* **1995**, *224*, 33. [[CrossRef](#)]
23. Medina, A.N.; Rojas, D.P.; Gandra, F.G.; Azanha, W.R.; Cardoso, L.P. Change of the Kondo regime in CePd_2Al_3 induced by chemical substitution: Verification of the Doniach diagram. *Phys. Rev. B* **1999**, *59*, 8738. [[CrossRef](#)]
24. Cornut, B.; Coqblin, B. Influence of the Crystalline Field on the Kondo Effect of Alloys and Compounds with Cerium Impurities. *Phys. Rev. B* **1972**, *5*, 11. [[CrossRef](#)]
25. Segal, E.; Wallace, E. Rare-earth ions in a hexagonal field I. *J. Solid State Chem.* **1970**, *2*, 347–365. [[CrossRef](#)]
26. García Soldevilla, J.; Gómez Sal, J.C.; Rodríguez, F.; Espeso, J.I.; Monconduit, L.; Allemand, J.; Paccard, D. Magnetic interactions competing in $\text{CeNi}_{1-x}\text{Cu}_x$ compounds. *Physica B* **1997**, *230*, 117–119. [[CrossRef](#)]
27. García Soldevilla, J.; Gómez Sal, J.C.; Espeso, J.I.; Rodríguez Fernández, J.; Blanco, J.A.; Fernández Díaz, M.T.; Buttner, H. Simultaneous changes of the 4f-conduction band hybridization and the density of states in the $\text{CeNi}_{1-x}\text{Cu}_x$ compounds. *J. Magn. Magn. Mater.* **1998**, *177*, 300–302. [[CrossRef](#)]
28. Andreica, D.; Amato, A.; Gygax, F.N.; Schenck, A. Nonmagnetic-magnetic transition in $\text{Yb}(\text{Cu}_{1-x}\text{Ni}_x)_2\text{Si}_2$ studied by muon-spin relaxation. *J. Phys. Cond. Matter* **2003**, *15*, 6997–7017. [[CrossRef](#)]
29. Cermáka, P.; Javorský, P.; Šantavá, E. Transition from Mixed-Valence to Trivalent Cerium State in $\text{Ce}(\text{Ni,Cu})\text{Al}$ series. *Acta Phys. Pol. A* **2010**, *118*, 926–928. [[CrossRef](#)]
30. Rojas, D.P.; Fernández Barquín, L.; Echevarria-Bonet, C.; Rodríguez Fernández, J. YbNi_2 : A heavy fermion ferromagnet. *Solid State Commun.* **2012**, *152*, 1834–1837. [[CrossRef](#)]